



Development of an empirical kinetic model for sonocatalytic process using neodymium doped zinc oxide nanoparticles



Alireza Khataee^{a,*}, Behrouz Vahid^b, Shabnam Saadi^a, Sang Woo Joo^{c,*}

^a Research Laboratory of Advanced Water and Wastewater Treatment Processes, Department of Applied Chemistry, Faculty of Chemistry, University of Tabriz, 51666-16471 Tabriz, Iran

^b Department of Chemical Engineering, Tabriz Branch, Islamic Azad University, 51579-44533 Tabriz, Iran

^c School of Mechanical Engineering, Yeungnam University, 712-749 Gyeongsan, South Korea

ARTICLE INFO

Article history:

Received 30 July 2015

Received in revised form 2 September 2015

Accepted 3 September 2015

Available online 14 September 2015

Keywords:

Kinetic modeling

Non-linear regression

ZnO nanoparticles

Sonocatalyst

Degradation

ABSTRACT

The degradation of Acid Blue 92 (AB92) solution was investigated using a sonocatalytic process with pure and neodymium (Nd)-doped ZnO nanoparticles. The nanoparticles were characterized by X-ray diffraction (XRD), scanning electron microscopy (SEM), and X-ray photoelectron spectroscopy (XPS). The 1% Nd-doped ZnO nanoparticles demonstrated the highest sonocatalytic activity for the treatment of AB92 (10 mg/L) with a degradation efficiency (DE%) of 86.20% compared to pure ZnO (62.92%) and sonication (45.73%) after 150 min. The results reveal that the sonocatalytic degradation followed pseudo-first order kinetics. An empirical kinetic model was developed using nonlinear regression analysis to estimate the pseudo-first-order rate constant (k_{app}) as a function of the operational parameters, including the initial dye concentration (5–25 mg/L), doped-catalyst dosage (0.25–1 g/L), ultrasonic power (150–400 W), and dopant content (1–6% mol). The results from the kinetic model were consistent with the experimental results ($R^2 = 0.990$). Moreover, DE% increases with addition of potassium periodate, peroxydisulfate, and hydrogen peroxide as radical enhancers by generating more free radicals. However, the addition of chloride, carbonate, sulfate, and t-butanol as radical scavengers declines DE%. Suitable reusability of the doped sonocatalyst was proven for several consecutive runs. Some of the produced intermediates were also detected by GC–MS analysis. The phytotoxicity test using *Lemna minor* (*L. minor*) plant confirmed the considerable toxicity removal of the AB92 solution after treatment process.

© 2015 Published by Elsevier B.V.

1. Introduction

The application of ultrasonic processes in advanced oxidation processes (AOPs) has been proposed recently for the treatment of various hazardous organic compounds, including halogenated hydrocarbons, pesticides components, and dyes in aqueous mediums [1–3]. Considerable amounts of dyes (up to 20%) can be lost in effluents during dyeing processes in the textile industry, which results in serious pollution of surface and ground waters that are resistant to biological treatment [4]. Sonication with a simple mechanism is an inexpensive solution to overcome this problem that can be used in ambient conditions.

The origin of the sonochemical effects is cavitation, which involves the generation, growth, and implosion of micro-bubbles within the liquid medium acting as localized micro-reactors

(a hot-spot approach). This collapse generates high temperature and pressure in the collapsing cavities and in the liquid immediately surrounding them (the interface area) [5,6]. Consequently, thermal cleavage of water occurs as the liquid and dissolved oxygen molecules produce reactive oxygen species (ROS), including $\cdot\text{O}_2^-$, $\cdot\text{O}$, $\cdot\text{OOH}$, and in particular $\cdot\text{OH}$ radicals. The hydroxyl radical ($\cdot\text{OH}$) as a strong oxidizing agent, reacts with pollutants effectively and unselectively to degrade them without generating secondary waste. [7,8].

However, the degradation rate of organic pollutants by ultrasonic processes is low, and complete mineralization rarely occurs [9,10]. To overcome these drawbacks, the ultrasonic method can be combined with Fe^{2+} , H_2O_2 , Fenton reagent, and semiconductor oxides to increase the production of $\cdot\text{OH}$ radicals [11,12]. For example, using appropriate catalysts (heterogeneous catalysis) like semiconductors (heterogeneous catalysis) can accelerate the sonochemical reactions by a synergistic effect of ultrasound and the solid semiconductor in the sonocatalytic process in an environmentally friendly coupled technique [8,9].

* Corresponding authors.

E-mail addresses: a_khataee@tabrizu.ac.ir, ar_khataee@yahoo.com (A. Khataee), swjoo@yu.ac.kr (S.W. Joo).

¹ Communicator.

Among the diverse catalysts, zinc oxide (ZnO) nanoparticles have attracted particular attention for properties such as a wide band gap (3.37 eV), high UV absorption potential, and high exciton binding energy (60 meV) [13]. Doping with rare-earth metals (REMs) is a practical way to increase the catalytic activity of ZnO by preventing fast recombination of the electron–hole pairs in the doped semiconductor [10,14]. The advantages of sonochemical methods for nanostructured material synthesis are the simple experimental conditions, quick procedure, and low cost compared to conventional methods [15].

Using intrinsic elementary reactions as a basis for a kinetic model is one of the best methods for model development because it involves exact understanding of the process reactions and the influences of the operational parameters [16–18]. However, this kind of modeling is sometimes difficult due to the diversity of reactions, particularly for coupled processes [19,20]. Empirical kinetic modeling of a process via non-linear regression analysis provides a nonlinear model that can be used for complicated combined AOPs, including photoelectro-Fenton and US/UV/H₂O₂ processes [19,21]. The validity of empirical modeling has been evaluated by comparing experimental and theoretically calculated data [22].

In this study, a simple sonochemical method was used to synthesize pure and Nd-doped ZnO nanoparticles. X-ray diffraction (XRD) and scanning electron microscopy (SEM) were used to characterize the prepared sonocatalysts. X-ray photoelectron spectroscopy (XPS) was used to confirm the presence of Nd in the catalyst structure. AB92 was treated as a model organic azo dye to determine the sonocatalytic activity of pure and Nd-doped ZnO nanoparticles, and the results were compared to those of sonolysis alone. To the best of our knowledge, sonocatalysis using Nd-doped ZnO nanoparticles for the degradation of AB92 has not been studied previously. Non-linear regression analysis was used to develop an empirical kinetic model considering the effect of the main operational parameters on k_{app} , including initial dye concentration, doped-catalyst dosage, ultrasonic power, and dopant content. The effects of various process enhancers and radical scavengers on the dye degradation efficiency (DE%) were studied. Finally, some of the intermediates generated during the sonocatalytic process were detected by GC–MS technique.

2. Materials and methods

2.1. Chemicals

All chemicals were analytical grade and used without further purification. ZnCl₂ was provided by Merck, Germany. Ethanol (C₂H₅OH, 99%) and neodymium chloride (NdCl₃·6H₂O) were purchased from Sigma Aldrich, USA. Acid Blue 92 (molecular formula = C₂₆H₁₆N₃Na₃O₁₀S₃, λ_{max} = 571 nm, M_w = 695.58 g/mol, color index number = 13,390), as an anionic monoazo dye, was obtained from Shimi Boyakhsaz Company (Iran).

2.2. Undoped ZnO and Nd-doped ZnO nanoparticles synthesis procedure

Undoped ZnO and Nd-doped ZnO nanoparticles were sonochemically synthesized as follows: (1) a molar pre-specified amount of NdCl₃·6H₂O was added to an aqueous solution of zinc chloride, (2) NaOH solution (1 M) was added dropwise to the prepared solution to set the pH to 10, (3) the obtained solution was sonicated for 3 h by an ultrasonic bath (Ultra 8060, England) with a frequency of 36 kHz, and (4) the resulting white crystalline product was washed with double distilled water and ethanol and dried at 80 °C for 12 h.

2.3. Characterization of nanocatalysts

XRD of the undoped and Nd-doped ZnO was conducted using a Siemens X-ray diffractometer (D8 Advance, Bruker, Germany) with Cu K_α radiation (λ = 1.54065 Å), an accelerating voltage of 40 kV, and an emission current of 30 mA. The surface morphology of the synthesized catalysts was investigated by SEM (TESCAN, MIRA3, Czech Republic), and a thermo scientific spectrometer (K-ALPHA, UK) was used for XPS measurements. The band gap of the nanocatalysts was measured by preparing a sample solution in distilled water and sonicating it for 20 min to obtain a homogeneous mixture. Microstructure distance-measurement software (Microstructure Measurement version 1.0) was applied to determine the size distribution of the as-prepared nanoparticles. The solution absorbance was recorded between 200 and 800 nm using an UV–Vis spectrophotometer (WPA lightwave S2000, England). Some of the intermediates during the sonocatalytic degradation of AB92 were detected by an Agilent 6890 gas chromatograph with a 30-m to 0.25-mm HP-5MS capillary column coupled with an Agilent 5973 mass spectrometer (Canada).

2.4. Sonocatalytic degradation of the dye

Sonocatalytic degradation experiments of AB92 were done for 150 min each using an ultrasonic bath (Ultra 8060, England) with a frequency of 36 kHz at the natural pH of the dye in the presence of various ZnO nanoparticles. A certain amount of nanocatalyst was added to 100 mL of AB92 solution with a specified concentration, and the prepared solution was sonicated in the dark to eliminate the photocatalysis effect. A typical sample of the ultrasonically treated solution was withdrawn at distinct process times, and the AB92 solution absorbance was measured using the UV–Vis spectrophotometer at its maximum absorbance wavelength (λ_{max} = 571 nm).

3. Results and discussion

3.1. Characterization of undoped ZnO and Nd-doped ZnO

Fig. 1 illustrates the X-ray diffraction patterns of pure and 1% Nd-doped ZnO nanoparticles. The main peaks were identified for undoped ZnO at 2θ of 31.92, 34.6, 36.48, 47.68, 56.72, 63, 66.08, 68, 68.28, 71.64, and 75.96, which are related to the (100), (002), (101), (102), (110), (103), (200), (112), (201), (004), and (202) planes of hexagonal wurtzite ZnO, respectively (JCPDS Card 36-1451) [23]. Identical peaks for the doped ZnO were seen without any diffraction peaks from neodymium oxides or other impurities. The diffraction values of the (100), (002), and (101) planes revealed a shift to lower angles in the case of Nd-doped ZnO compared to pure ZnO, indicating appropriate doping of Nd ions into the ZnO lattice. This shift can be explained by the expansion of the ZnO lattice through doping by neodymium due to the larger ionic radius of Nd³⁺ (0.983 Å) in comparison with Zn²⁺ (0.74 Å).

Fig. 2a and b demonstrate SEM images of the undoped ZnO and 1% Nd-doped ZnO nanoparticles, respectively. Fig. 2a shows that the undoped ZnO nanoparticles are irregular in shape and size in comparison with the Nd-doped ZnO nanoparticles, which is related to the growth of irregular crystalline grains during the synthesis and their aggregation. Fig. 2b shows that the incorporation of Nd into the crystal structure of ZnO can decrease the aggregation phenomenon and hence reduce the size of nanoparticles and improve the shape uniformity of them. The presence of the Nd dopant decreases the crystal size of Nd-doped ZnO sample, which was mainly attributed to the generation of Nd–O–Zn on the surface of

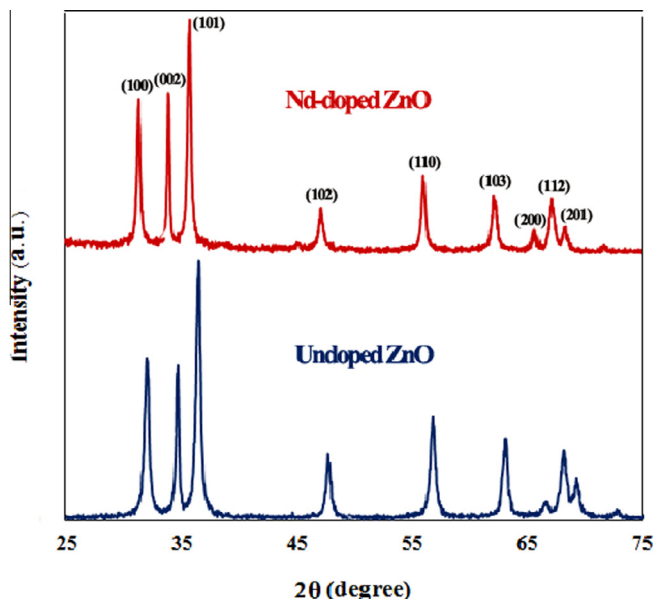


Fig. 1. XRD patterns of undoped and 1% Nd-doped ZnO nanoparticles.

the catalyst preventing the growth of crystal grains [24]. Moreover, sonochemical synthesis of the catalyst generally results in de-aggregation of the synthesized nanoparticles and hence good spherical shape of the doped nanoparticles observed owing to their lower crystalline size. Also, the de-aggregation of the particles provides more active sites for the reaction [25]. Fig. 2c shows that the major size distribution of the 1% Nd-doped particles was in the range of 40–60 nm with a frequency of 67.5%.

Fig. 3 illustrates the XPS spectra of the 1% Nd-doped ZnO nanoparticles, and it is clear that there are Zn, O, C, and Nd peaks on the surface of the catalyst. The corresponding energies of these elements are given in Table 1. The O_{1s} , C_{1s} , $Zn_{2p_{3/2}}$, and $Zn_{2p_{1/2}}$ binding energies are close to 532.08, 286.08, 1023.08, and 1046.08 eV, respectively, which corresponds to the wurtzite structure of the hexagonal zinc (II) oxide [26]. It should be stated that the other binding energies which are observed at 11.08, 92.08, 141.08 and 1198.08 eV are attributed to Zn_{3d} , Zn_{3p} , Zn_{3s} and Zn_{2s} , respectively. Also, the specified area in the Fig. 3 is ascribed to Auger Zn LMM peaks [27–29].

Fig. 3 also depicts the spectra of the Nd 3d core level photoemission are located at 1004.98 and 984.08 eV, respectively, and are in good agreement with the $Nd_{3d_{3/2}}$ and $Nd_{3d_{5/2}}$ peaks. This shows that the Nd ions exist in a trivalent state based on literature data for Nd ions in Nd_2O_3 [30].

The band gap of the ZnO semiconductor was calculated using Eq. (1) [31]:

$$(Ah\nu)^2 = K(h\nu - E_g) \quad (1)$$

where $h\nu$ is the energy of a photon (eV), A is the absorption, K is a constant, and E_g is the band gap. The band gap can be determined by extrapolating the linear region in the diagram of $(Ah\nu)^2$ against the photon energy (Fig. 4). The band gap values of 3.20, 2.60, 2.80, 2.85 and 2.90 eV were obtained for the undoped ZnO, 1%, 2%, 4% and 6% Nd-doped ZnO nanoparticles, respectively

3.2. Comparison of sonolysis and sonocatalysis processes

AB92 adsorption on the ZnO catalysts (approximately 7% after 60 min) can be neglected for removal from the solution. The

degradation of AB92 (10 mg/L) was compared under sonication in the presence and absence of ZnO nanoparticles at identical operational conditions in 150 min of treatment (Fig. 5). The results revealed that DE% was 45.73%, 62.9%, and 86.20% for sonolysis, sonocatalysis with undoped ZnO, and sonocatalysis with Nd-doped ZnO nanoparticles, respectively. Combining semiconductor catalysts with sonolysis enhances the performance of the ultrasound process by formation of electron–hole pairs after excitation of the electrons from the valence to conduction band. Then, interface oxidation of the adsorbed hydroxyl anions and water molecules occurs on the catalyst surface as a result of the holes, which generates $\cdot OH$ radicals. Interaction of the conduction-band electrons with adsorbed oxygen molecules produces $\cdot O_2^-$ and $\cdot OOH$ radicals, which can oxidize the contaminants (Eqs. (2)–(6)) [32,33].

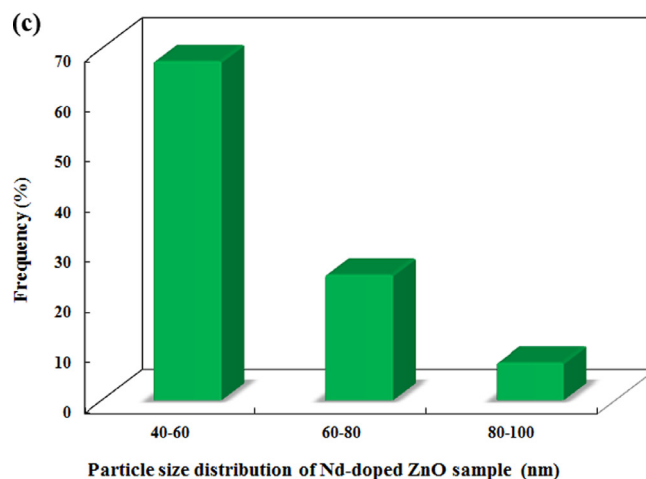
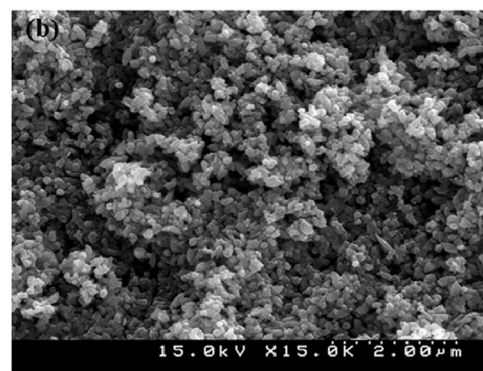
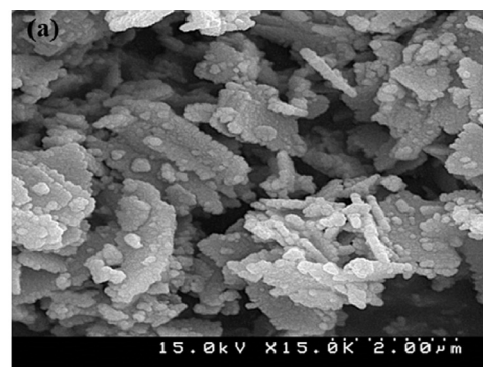


Fig. 2. SEM images of (a) undoped ZnO, (b) 1% Nd-doped ZnO, and (c) 1% Nd-doped ZnO particle size distribution.

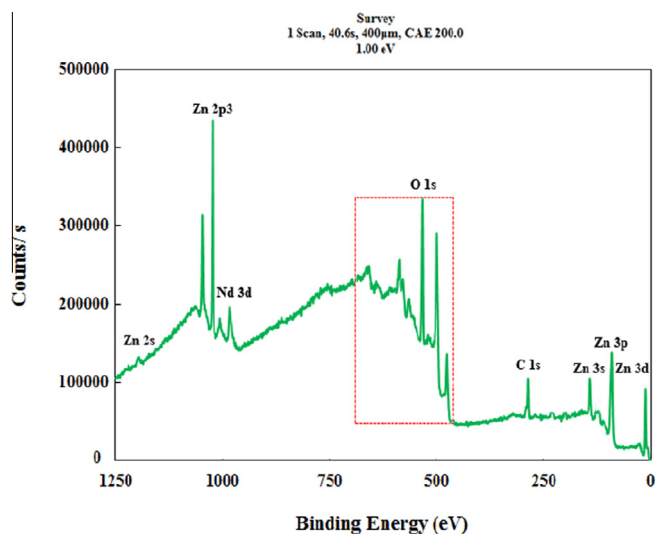
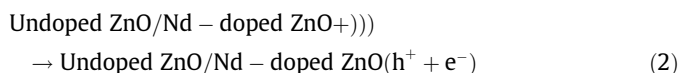


Fig. 3. XPS spectra of 1% Nd-doped ZnO nanoparticles.



More holes can also be produced by an oxygen escape mechanism where some surface oxygen atoms escape from the crystal lattice as a result of strong shock waves generated by cavitation bubbles during their collapse [34]. Furthermore, catalyst crevices containing entrapped gas act as a cavitation nucleus and lower the tensile strength of the solid–liquid interface compared to the bulk liquid, which generates more active cavitation bubbles. A sonoluminescence phenomenon also occurs, and the small activity of the semiconductor as a photocatalyst cannot be eliminated [35]. Rare earth ion doping into the pure ZnO lattice also creates impurity energy levels in the band gap and produces traps for the generated charge carriers. This accelerates the interfacial charge transfer and inhibits the recombination of electron–hole pairs [36,37]. Finally, the ultrasonic waves not only increase the active surface area of the sonocatalyst by de-aggregation but also enhance the mass transfer of various species from the solution to the semiconductor surface [38].

The rest of the experiments were carried out using sonocatalysis with the Nd-doped ZnO catalyst. AB92 is a non-volatile and

Table 1

Location of Zn, C 1s, O 1s and Nd 3d peaks in the XPS spectrum of Nd-doped ZnO.

Nd-doped ZnO	
Peak	Binding energy (eV)
Zn _{2s}	1198.08
Zn _{2p1/2}	1046.08
Zn _{2p3/2}	1023.08
Zn _{3s}	141.08
Zn _{3p}	92.08
Zn _{3d}	11.08
O _{1s}	532.08
Nd _{3d5/2}	984.08
Nd _{3d3/2}	1004.98
C _{1s}	286.08

water-soluble compound, so its presence in the gaseous phase of a cavity is not likely [39]. As a consequence, the main routes for AB92 degradation are chemical oxidation by ROS, especially hydroxyl radicals in the interfacial area of the gas and bulk solution and on the surface of the sonocatalyst [40].

3.3. Kinetic of sonocatalytic degradation using Nd-doped ZnO and modeling of operational parameters

The operational conditions of the sonocatalytic process for empirical kinetic modeling are summarized in Table 2. According to the pseudo-first-order kinetic assumption from the slope of $\ln(C_0/C)$ against time (t), k_{app} was estimated for each experiment with high correlation coefficients (R^2), which were greater than 0.99, thus confirming the suggested kinetic. The non-linear relation of k_{app} with each of the operational parameters can be separately modeled by an empirical power law equation for the initial dye concentration, doped-catalyst dosage, ultrasonic power, and dopant content (Eq. (7)) [41]:

$$k_{app} = \alpha(\text{operational parameter})^\beta \quad (7)$$

The model constants α and β were calculated by non-linear regression analysis of the experimental results, and the results are shown in Figs. 6–9.

k_{app} and thus DE% were increased by increasing the catalyst dosage (Fig. 6) and ultrasound power (Fig. 7) during the 150-min process time. The effect of catalyst dosage is attributed to the greater available surface area with active reaction sites, which increases the production of hydroxyl radicals for the AB92 degradation [42]. However, after an optimum value of 1 g/L, DE% decreases due to nanoparticle aggregation and ultrasound scattering, which decreases the active sites and blocks the transmission of ultrasound waves, respectively [13,43].

The ultrasound power is an important instrumental parameter that affects the cavitation activity [44]. The improvement of DE % with the ultrasonic power is due to the greater formation of collapsing bubbles. This enhances the formation of $\cdot\text{OH}$ radicals and increases the degradation of target contaminants [10,44]. Furthermore, at elevated ultrasound power, the turbulence of the solution increased, which increased the mass transfer rate of the dye, the generated intermediates, and the reactive radicals between the solution and the catalyst surface. The available active sites on the surface of the catalyst are also increased by increased de-aggregation [45,46].

k_{app} and DE% were decreased by increasing the initial concentration of AB92 (Fig. 8) and the dopant content (Fig. 9) during the 150-min process time. At identical operational conditions,

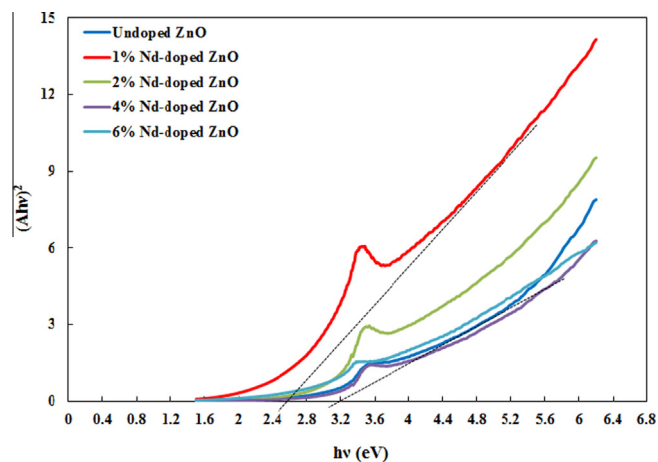


Fig. 4. $(Ah\nu)^2 - h\nu$ curves of the undoped and 1%Nd-doped ZnO nanoparticles.

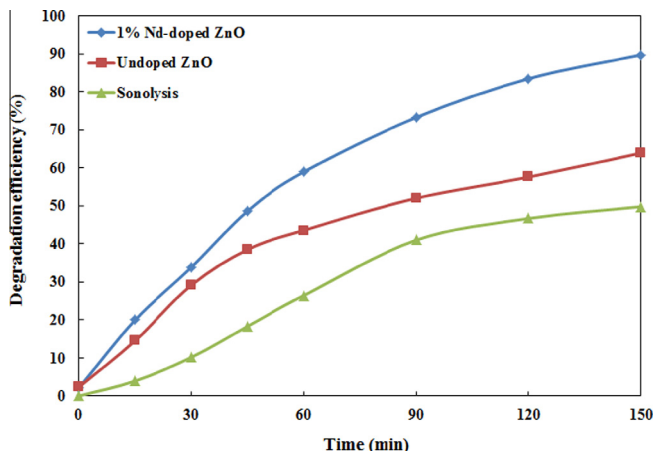


Fig. 5. Comparison of different processes in the degradation of AB92. Initial dye concentration = 10 mg/L, catalyst dosage = 1 g/L and ultrasonic power = 150 W.

the number of generated hydroxyl radicals is constant, and these radicals have to react with more dye and degradation intermediates [10]. Hence, the sonocatalytic process is more promising at a lower concentration of contaminants [47].

The enhanced sonocatalytic activity by incorporation of Nd can be explained by two mechanisms. Firstly, the presence of Nd in the ZnO lattice can alter the absorbance properties of the catalyst. Based on this mechanism, the sonocatalyst band gap has a significant role in the sonocatalysis [31,48]. As mentioned in Section 3.1, the band gap of Nd-doped ZnO nanoparticles decreases compared to pure ZnO because of the formation of a shallow level inside the band gap. As a result, the transition from the ground to the excited state is easier with the narrower band gaps.

Moreover, Nd^{3+} acts as an electron scavenger and prevents electron-hole pairs recombination [49,50]. However, appropriate loading of Nd^{3+} ions is important for generating a significant potential difference between the surface and the center of the nanoparticles to separate the electron-hole pairs effectively. This loading was chosen as 1% of Nd. Excess dopant covers the surface of ZnO nanoparticles and decreases the sonocatalytic activity by increasing the space charge layer in the ZnO lattice and consequently accelerating the electron-hole pair recombination rate [10,24,51].

3.4. Development and evaluation of empirical kinetic model

As mentioned, the degradation of AB92 obeys pseudo-first-order kinetics. k_{app} is a function of the operational parameters as follows (Eq. (8)):

$$k_{\text{app}} = k' \frac{[\text{Doped - catalyst}]^a (\text{US power})^b}{[\text{AB92}]^c (\text{Dopant content})^d} \quad (8)$$

Non-linear analysis regression was used to estimate a , b , c , and d . Then, k' could be calculated for each run using known values of k_{app} , the initial AB92 concentration, the amount of doped catalyst, ultrasound power, and dopant content applied in each experiment. The mean value of k' was obtained as 0.0026.

Table 2

The operational conditions of sonocatalytic process.

Parameter	Range
Catalyst dosage (g/L)	0.25–1
Ultrasonic power (W)	150–400
Initial AB92 concentration (mg/L)	5–25
Dopant content (%)	1–6

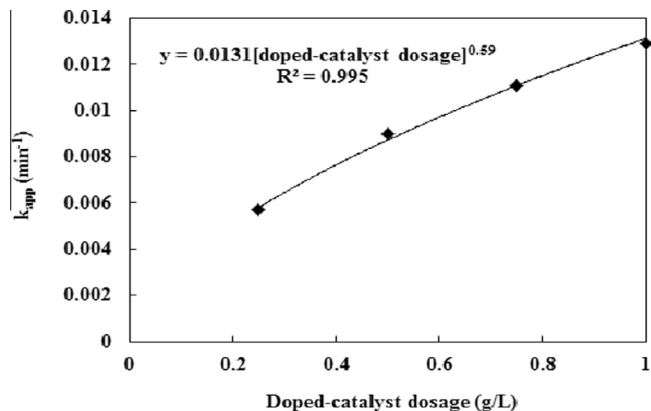


Fig. 6. The effect of catalyst dosage on k_{app} . Initial dye concentration = 10 mg/L, dopant content = 1%, and ultrasonic power = 150 W.

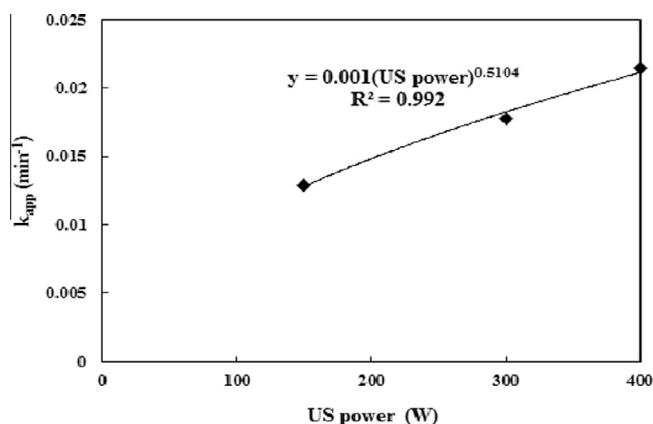


Fig. 7. The effect of ultrasonic power on k_{app} . Dopant content = 1%, catalyst dosage = 1 g/L and initial dye concentration = 10 mg/L.

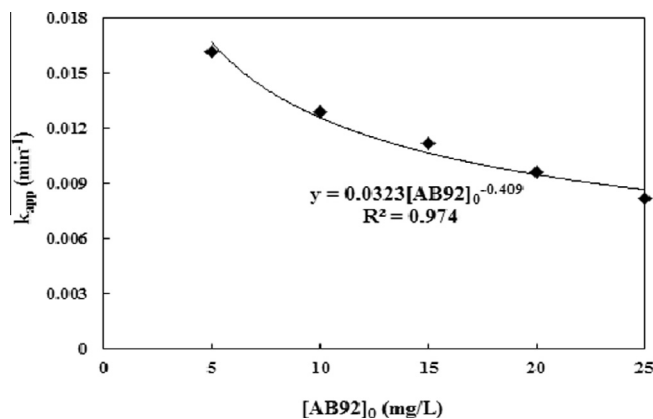


Fig. 8. The effect of AB92 initial concentration on k_{app} . Dopant content = 1%, catalyst dosage = 1 g/L and ultrasonic power = 150 W.

By substituting the estimated values into Eq. (8), Eq. (9) was obtained as the empirical kinetic model for prediction of k_{app} in different experimental conditions:

$$k_{\text{app}} = 0.0026 \frac{[\text{Doped - catalyst}]^{0.59} (\text{US power})^{0.5104}}{[\text{AB92}]^{0.409} (\text{Dopant percentage})^{0.177}} \quad (9)$$

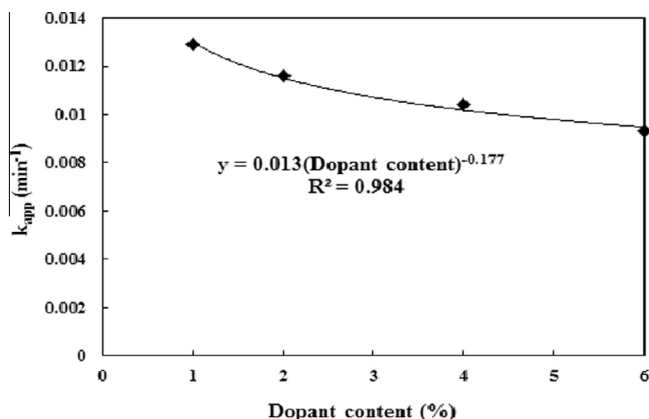


Fig. 9. The effect of dopant content on k_{app} . Initial dye concentration = 10 mg/L, catalyst dosage = 1 g/L and ultrasonic power = 150 W.

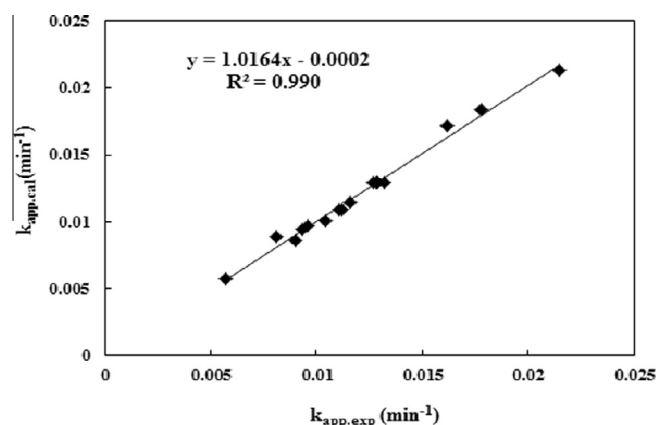
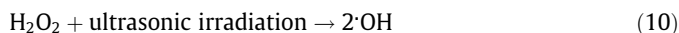


Fig. 10. Comparison between experimental and calculated pseudo-first order rate constants (min^{-1}) for degradation of AB92 in the sonocatalytic process at different operational condition. For experimental details refer to Table 3.

The experimental and calculated k_{app} for degradation of AB92 (Table 3) were compared to evaluate the obtained empirical kinetic model in Fig. 10, which shows a good agreement of the model and the experimental results ($R^2 = 0.990$).

3.5. Effect of enhancers

The effect on DE% was measured for enhancers such as hydrogen peroxide, peroxydisulfate, and potassium periodate with initial concentrations of 0.15 mM. The results are plotted in Fig. 11. The enhancers increase the AB92 sonocatalytic degradation from 86.20% to 90.08%, 92.50%, and 94.65%, respectively. For hydrogen peroxide, the enhanced degradation of the dye is mainly due to the excess production of $\cdot\text{OH}$ radicals by the ultrasound (Eq. (10)). Hydrogen peroxide also promotes the formation rate of $\cdot\text{OH}$ radicals by reduction in the conduction band (Eq. (11)) [42,52].



The addition of peroxydisulfate can also enhance DE% due to the production of sulfate radicals, which react with water to form extra $\cdot\text{OH}$ radicals (Eqs. (12)–(15)) [1]:

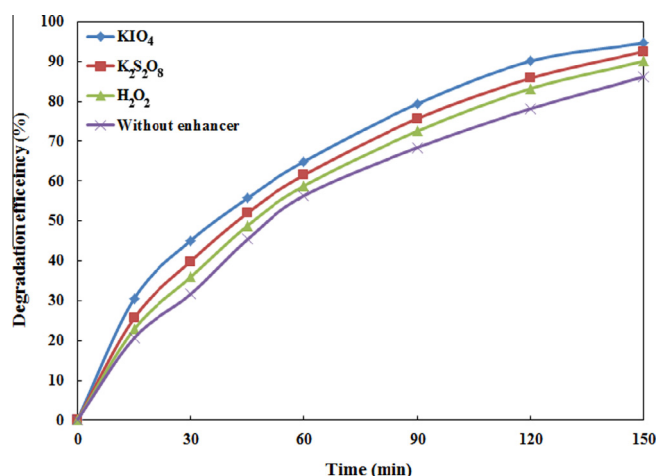
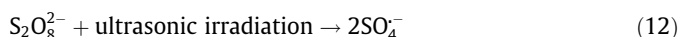


Fig. 11. Effect of enhancers on the sonocatalytic degradation of AB92. Dopant content = 1%, initial dye concentration = 10 mg/L, enhancer concentration = 0.15 mmol/L, catalyst dosage = 1 g/L and ultrasonic power = 150 W.

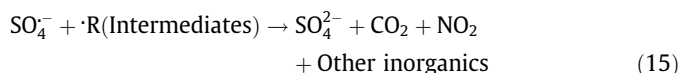


Table 3

Apparent pseudo-first-order rate constants of the sonocatalytic process at different operational conditions.

[AB92] ₀ (mg/L)	[doped-catalyst] (g/L)	US power (W)	Dopant content (%)	$k_{app-exp}$ (min^{-1})	$k_{app-cal}$ (min^{-1})
10	0.25	150	1	0.0057	0.0057
10	0.5	150	1	0.009	0.0086
10	0.75	150	1	0.0111	0.0109
10	1	150	1	0.0129	0.0129
5	1	150	1	0.0162	0.0171
15	1	150	1	0.0112	0.0109
20	1	150	1	0.0096	0.0097
25	1	150	1	0.0082	0.0089
10	1	300	1	0.0178	0.0184
10	1	400	1	0.0215	0.0213
10	1	150	2	0.0116	0.0114
10	1	150	4	0.0104	0.0101
10	1	150	6	0.0093	0.0094
10	1	150	1	0.0129	0.0129
10	1	150	1	0.0128	0.0129
10	1	150	1	0.0127	0.0129

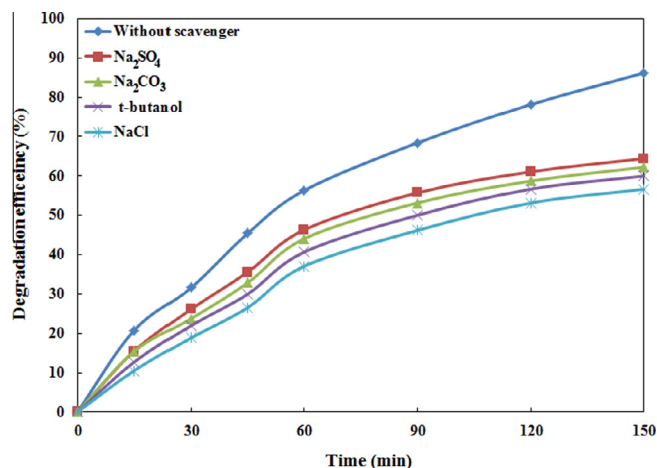


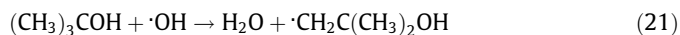
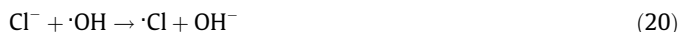
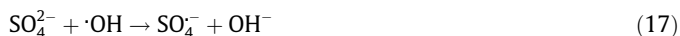
Fig. 12. Differing sonocatalytic degradation efficiency at the presence of various radical scavengers. Dopant content = 1%, catalyst dosage = 1 g/L, initial dye concentration = 10 mg/L, scavenger concentration = 100 mg/L and ultrasonic power = 150 W.

Potassium periodate addition produces the most favorable effect on DE% among the enhancers due to electron capture from the conduction band (Eq. (16)) [53]:



3.6. Effect of radical scavengers

The effect of various anions and organic compounds on the sonocatalytic process is significant from a practical point of view because of their possible presence in real wastewater and their role as radical scavengers. Hence, sodium sulfate, sodium carbonate, sodium chloride, and t-butanol were selected with an initial concentration of 100 mg/L to evaluate the influence on DE%. Fig. 12 shows an inhibiting effect on the sonocatalytic degradation of AB92 for all of the radical scavengers, confirming the free radical attack mechanism for the treatment process. The possible reactions that can occur in the presence of the radical scavengers are as follows (Eqs. (17)–(22)) [44,54]:



Experiments were performed at pH 6 (the natural pH of dye), which is below the zero charge point of the ZnO nanoparticles ($\text{pH}_{\text{zcp}} = 9.0$) [14]. The positively charged ZnO nanoparticles attract the negatively charged anions electrostatically, and as a consequence, the reaction of generated holes with the adsorbed anions reduces the $\cdot\text{OH}$ radical formation. The active sites of the sonocatalyst occupied by these anions deactivate the sonocatalyst surface for the dye and the adsorption of degradation intermediates, which react with adsorbed hydroxyl radicals and result in lower DE% [32]. The data suggest that $\cdot\text{OH}$ radicals have an essential function in the sonocatalytic process. Similar data have been reported for the sonocatalytic degradation of methylene blue dye [7].

3.7. Reusability of the sonocatalyst

Consecutive application of the sonocatalyst while maintaining its activity is critical for practical use. It has been proven that catalyst doping with an appropriate dopant enhances its reusability [49]. Therefore, a reusability test for the 1% Nd-doped ZnO nanocatalyst was performed for the AB92 (10 mg/L) treatment (Fig. 13). The data demonstrated negligible drops in DE% within four repeated cycles to 86.20%, 86.01%, 85.81%, and 84.67%, respectively. These data revealed that the 1% Nd-doped ZnO nanoparticles are durable and effective for the remediation of colored wastewaters.

3.8. AB92 degradation intermediates

The intermediates generated during the sonocatalytic degradation process were analyzed by GC–MS and identified by matching their spectra with commercial standards recorded in the Mass library (Wiley 7n) to find match factors above 90% [55]. Molecular structure and retention time of four detected components after 6 min of degradation are shown in Table 4. Generation of these intermediates during the decolorization of AB92 confirmed active degradation of this pollutant through the sonocatalytic degradation process.

3.9. Phytotoxicity assessment

Phytotoxicity is defined as the compound capacity to cause damage to an aquatic plant. In this research, the phytotoxicity of solutions containing 10 mg/L of AB92 and 1 g/L of 1% Nd-doped ZnO sample was investigated according to our previous work [56]. For the phytotoxicity experiment, twenty fully-grown fronds of *Lemna minor* (*L. minor*) were carried to a 200 mL beaker containing 100 mL of tested solution and 2 mL of growth medium. The tested solutions were selected as water, AB92 solution and treated AB92 solution after the separation of the doped nanoparticles, respectively. Relative frond number was calculated through Eq. (23):

$$\text{Relative frond number (RFN)} = \frac{(\text{frond } N_7 - \text{frond } N_0)}{\text{frond } N_0} \quad (23)$$

where N_0 and N_7 are the number of fronds on days 0 and 7, respectively. The RFN was calculated as 0.7, 0.3 and 0.6 for the above mentioned tested solutions, respectively. RFN was smaller in the AB92

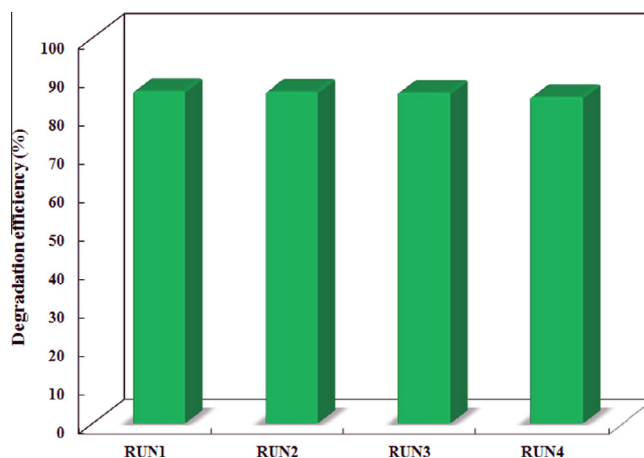
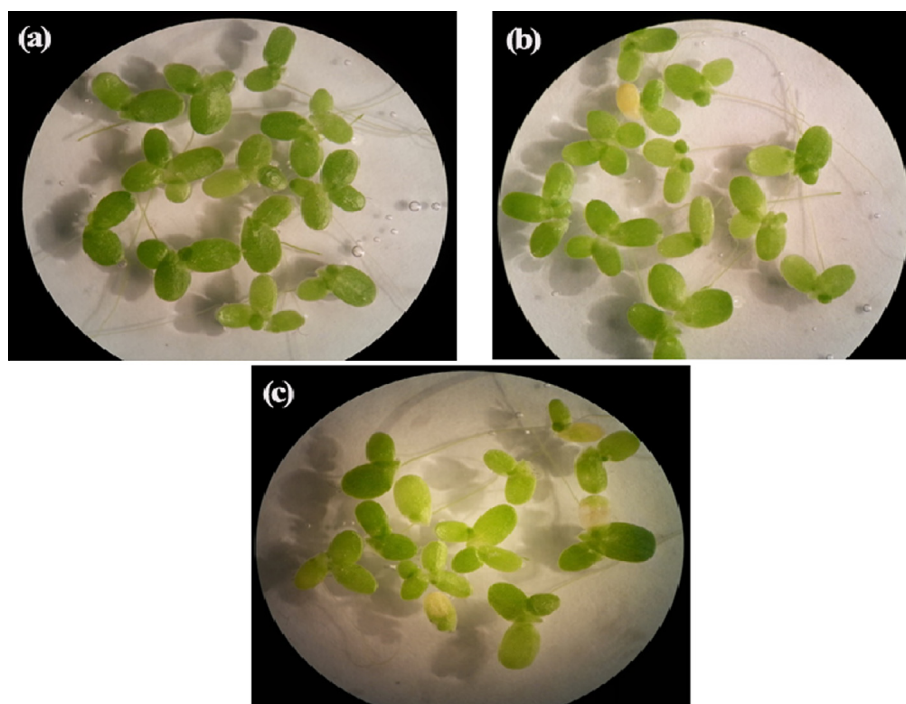


Fig. 13. Reusability of the 1% Nd-doped ZnO nanoparticles within 4 consecutive experimental runs. Dopant content = 1%, catalyst dosage = 1 g/L, initial dye concentration = 10 mg/L, reaction time = 150 min and ultrasonic power = 150 W.

Table 4
Identified intermediates during sonocatalytic degradation of Acid Blue 92.

No.	Structure	t_R (min)	Main fragments (m/z)	Compound
1		31.424	149.00 (100.00%), 57.10 (44.43%), 167.00 (38.82%), 55.00 (35.49%), 207.00 (33.46%)	1,2-Benzenedicarboxylic acid
2		2.285	75.00 (100.00%), 117.00 (58.55%), 73.00 (12.09%), 76.00 (7.62%), 118.00 (5.80%)	Acetic acid
3		4.681	75.00 (100.00%), 116.00 (75.43%), 73.00 (13.26%), 76.00 (7.56%), 117.00 (7.48%)	Acetamide
4		2.684	59.00 (100.00%), 60.00 (2.55%), 57.10 (0.5%), 55.10 (0.41%), 71.10 (0.36%)	Methylformamide

**Fig. 14.** Macroscopic images of *L. minor* (a) control sample, (b) treated AB92 solution and (c) AB92 solution.

solution compared to the control and treated samples (Fig. 14), which indicates that the toxicity of the AB92 solution was more than other samples. After treatment of the AB92 solution, RFN increases from 0.3 to 0.6, which shows the toxicity reduces owing to the effectively degradation of the dye. However, it is yet less than the control sample, which can be attributed to the incomplete dye degradation (DE% = 86.20%) after 150 min of treatment.

4. Conclusion

Sonochemically prepared Nd-doped ZnO nanoparticles were applied as a sonocatalyst for the degradation of AB92 azo dye in

aqueous solution. XRD patterns demonstrated that the particles were crystallized in a hexagonal wurtzite lattice. SEM images revealed that the incorporation of Nd into the ZnO crystal structure prevents particle aggregation. XPS spectra confirmed the presence of Nd in the doped samples. Based on the obtained results, DE% for the sonocatalysis with doped catalysts was higher than sonocatalysis with undoped catalyst and sonolysis alone. Furthermore, DE% was influenced by the dopant content, and 1% Nd-doped ZnO nanoparticles were selected as the most effective catalyst in the other experiments. DE% was noticeably affected by experimental parameters like the catalyst dosage, initial AB92 concentration, dopant content, and ultrasound power. The addition of enhancers

and radical scavengers accelerated and reduced DE%, respectively, indicating that free radicals are the predominant controlling mechanism for sonochemical degradation. Also, the sonocatalyst demonstrated high durability after four consecutive experiments, and some of the degradation intermediates were recognized by GC–MS analysis. Finally, by applying a nonlinear regression analysis, an empirical kinetic model was developed for calculating k_{app} under various operational conditions. The experimental data for k_{app} were consistent with calculated data ($R^2 = 0.990$), which validated the empirical kinetic model. The phytotoxicity studies demonstrated the remarkable toxicity removal from the AB92 solution after treatment by the sonocatalytic process.

Acknowledgement

The authors thank the University of Tabriz (Iran) for all the support and guidance. This work is funded by the grant NRF-2015-002423 of the National Research Foundation of Korea.

References

- [1] A. Khataee, S. Saadi, M. Safarpour, S.W. Joo, Sonocatalytic performance of Er-doped ZnO for degradation of a textile dye, *Ultrason. Sonochem.* (2015).
- [2] A. Khataee, Optimization of UV-promoted peroxydisulphate oxidation of CI Basic Blue 3 using response surface methodology, *Environ. Technol.* 31 (2010) 73–86.
- [3] M. Kasiri, A. Khataee, Photooxidative decolorization of two organic dyes with different chemical structures by UV/H₂O₂ process: experimental design, *Desalination* 270 (2011) 151–159.
- [4] R. Marandi, M. Khosravi, M. Olya, B. Vahid, M. Hatami, Photocatalytic degradation of an azo dye using immobilised TiO₂ nanoparticles on polyester support: central composite design approach, *Micro Nano Lett.* IET 6 (2011) 958–963.
- [5] Y.-C. Chen, P. Smirniotis, Enhancement of photocatalytic degradation of phenol and chlorophenols by ultrasound, *Ind. Eng. Chem. Res.* 41 (2002) 5958–5965.
- [6] K. Suslick, S. Doktycz, E. Flint, On the origin of sonoluminescence and sonochemistry, *Ultrasonics* 28 (1990) 280–290.
- [7] N. Shimizu, C. Ogino, M.F. Dadjour, T. Murata, Sonocatalytic degradation of methylene blue with TiO₂ pellets in water, *Ultrason. Sonochem.* 14 (2007) 184–190.
- [8] S. Anju, K. Jyothi, S.Y. Sindhu Joseph, E. Yesodharan, Ultrasound assisted semiconductor mediated catalytic degradation of organic pollutants in water: comparative efficacy of ZnO, TiO₂ and ZnO–TiO₂, *Res. J. Recent Sci.* 2277 (2012) 2502.
- [9] J. Wang, Z. Jiang, Z. Zhang, Y. Xie, Y. Lv, J. Li, Y. Deng, X. Zhang, Study on inorganic oxidants assisted sonocatalytic degradation of Acid Red B in presence of nano-sized ZnO powder, *Sep. Purif. Technol.* 67 (2009) 38–43.
- [10] A. Khataee, A. Karimi, S. Arefi-Oskoui, R.D.C. Soltani, Y. Hanifehpour, B. Soltani, S.W. Joo, Sonochemical synthesis of Pr-doped ZnO nanoparticles for sonocatalytic degradation of Acid Red 17, *Ultrason. Sonochem.* 22 (2015) 371–381.
- [11] I. Ioan, S. Wilson, E. Lundanes, A. Neculai, Comparison of Fenton and sono-Fenton bisphenol A degradation, *J. Hazard. Mater.* 142 (2007) 559–563.
- [12] M. Bertelli, E. Selli, Kinetic analysis on the combined use of photocatalysis, H₂O₂ photolysis, and sonolysis in the degradation of methyl tert-butyl ether, *Appl. Catal. B* 52 (2004) 205–212.
- [13] A. Khataee, R.D.C. Soltani, A. Karimi, S.W. Joo, Sonocatalytic degradation of a textile dye over Gd-doped ZnO nanoparticles synthesized through sonochemical process, *Ultrason. Sonochem.* 23 (2015) 219–230.
- [14] R. Darvishi Cheshmeh Soltani, A. Rezaee, A. Khataee, Combination of carbon black–ZnO/UV process with an electrochemical process equipped with a carbon black–PTFE-coated gas-diffusion cathode for removal of a textile dye, *Ind. Eng. Chem. Res.* 52 (2013) 14133–14142.
- [15] O. Yayapao, T. Thongtem, A. Phuruangrat, S. Thongtem, Sonochemical synthesis of Dy-doped ZnO nanostructures and their photocatalytic properties, *J. Alloy. Compd.* 576 (2013) 72–79.
- [16] J.P. Pocostales, P.M. Alvarez, F.J. Beltrán, Kinetic modeling of powdered activated carbon ozonation of sulfamethoxazole in water, *Chem. Eng. J.* 164 (2010) 70–76.
- [17] L. Qin, Y.-L. Lin, B. Xu, C.-Y. Hu, F.-X. Tian, T.-Y. Zhang, W.-Q. Zhu, H. Huang, N.-Y. Gao, Kinetic models and pathways of ronidazole degradation by chlorination, UV Irradiat. UV/Chlorine Processes *Water Res.* 65 (2014) 271–281.
- [18] L.J. Xu, W. Chu, N. Graham, Sonophotolytic degradation of dimethyl phthalate without catalyst: analysis of the synergistic effect and modeling, *Water Res.* 47 (2013) 1996–2004.
- [19] A. Khataee, B. Vahid, B. Behjati, M. Safarpour, S.W. Joo, Kinetic modeling of a triarylmethane dye decolorization by photoelectro-Fenton process in a recirculating system: nonlinear regression analysis, *Chem. Eng. Res. Des.* 92 (2014) 362–367.
- [20] A.R. Khataee, M. Fathinia, M. Zarei, B. Izadkhah, S.W. Joo, Modeling and optimization of photocatalytic/photoassisted-electro-Fenton like degradation of phenol using a neural network coupled with genetic algorithm, *J. Ind. Eng. Chem.* 20 (2014) 1852–1860.
- [21] M.A. Behnajady, B. Vahid, N. Modirshahla, M. Shokri, Evaluation of electrical energy per order (EEO) with kinetic modeling on the removal of Malachite Green by US/UV/H₂O₂ process, *Desalination* 249 (2009) 99–103.
- [22] L.G. Devi, K. Rajashekhar, K.A. Raju, S.G. Kumar, Kinetic modeling based on the non-linear regression analysis for the degradation of Alizarin Red S by advanced photo Fenton process using zero valent metallic iron as the catalyst, *J. Mol. Catal. A Chem.* 314 (2009) 88–94.
- [23] R. Wang, J.H. Xin, Y. Yang, H. Liu, L. Xu, J. Hu, The characteristics and photocatalytic activities of silver doped ZnO nanocrystallites, *Appl. Surf. Sci.* 227 (2004) 312–317.
- [24] M. Khatamian, A. Khandar, B. Divband, M. Haghghi, S. Ebrahimi, Heterogeneous photocatalytic degradation of 4-nitrophenol in aqueous suspension by Ln (La³⁺, Nd³⁺ or Sm³⁺) doped ZnO nanoparticles, *J. Mol. Catal. A Chem.* 365 (2012) 120–127.
- [25] N. Ghows, M.H. Entezari, Exceptional catalytic efficiency in mineralization of the reactive textile azo dye (RB5) by a combination of ultrasound and core-shell nanoparticles (CdS/TiO₂), *J. Hazard. Mater.* 195 (2011) 132–138.
- [26] M. Chen, X. Wang, Y. Yu, Z. Pei, X. Bai, C. Sun, R. Huang, L. Wen, X-ray photoelectron spectroscopy and Auger electron spectroscopy studies of Al-doped ZnO films, *Appl. Surf. Sci.* 158 (2000) 134–140.
- [27] E. Antonides, E. Janse, G. Sawatzky, LMM Auger spectra of Cu, Zn, Ga, and Ge. I. Transition probabilities, term splittings, and effective Coulomb interaction, *Phys. Rev. B* 15 (1977) 1669.
- [28] G. Deroubaix, P. Marcus, X-ray photoelectron spectroscopy analysis of copper and zinc oxides and sulphides, *Surf. Interface Anal.* 18 (1992) 39–46.
- [29] M. Futsuhara, K. Yoshioka, O. Takai, Structural, electrical and optical properties of zinc nitride thin films prepared by reactive rf magnetron sputtering, *Thin Solid Films* 322 (1998) 274–281.
- [30] J. Zheng, J. Song, Z. Zhao, Q. Jiang, J. Lian, Optical and magnetic properties of Nd-doped ZnO nanoparticles, *Cryst. Res. Technol.* 47 (2012) 713–718.
- [31] S. Farhadi, K. Pourzare, S. Sadeghinejad, Synthesis and characterization of Co₃O₄ nanoparticles by simple thermolysis of the [Co(NH₃)₆]₂(C₂O₄)₃·4H₂O complex, *Polyhedron* 67 (2014) 104–110.
- [32] S. Anju, S. Yesodharan, E. Yesodharan, Zinc oxide mediated sonophotocatalytic degradation of phenol in water, *Chem. Eng. J.* 189 (2012) 84–93.
- [33] A. Khataee, M. Sheydaei, A. Hassani, M. Taseidifar, S. Karaca, Sonocatalytic removal of an organic dye using TiO₂/Montmorillonite nanocomposite, *Ultrason. Sonochem.* 22 (2015) 404–411.
- [34] H. Salavati, N. Tavakkoli, M. Hosseinpoor, Preparation and characterization of polyphosphotungstate/ZrO₂ nanocomposite and their sonocatalytic and photocatalytic activity under UV light illumination, *Ultrason. Sonochem.* 19 (2012) 546–553.
- [35] E. Selli, Synergistic effects of sonolysis combined with photocatalysis in the degradation of an azo dye, *Phys. Chem. Chem. Phys.* 4 (2002) 6123–6128.
- [36] O. Yayapao, T. Thongtem, A. Phuruangrat, S. Thongtem, Ultrasonic-assisted synthesis of Nd-doped ZnO for photocatalysis, *Mater. Lett.* 90 (2013) 83–86.
- [37] J.-C. Sin, S.-M. Lam, K.-T. Lee, A.R. Mohamed, Preparation and photocatalytic properties of visible light-driven samarium-doped ZnO nanorods, *Ceram. Int.* 39 (2013) 5833–5843.
- [38] Y. Zhai, Y. Li, J. Wang, J. Wang, L. Yin, Y. Kong, G. Han, P. Fan, Effective sonocatalytic degradation of organic dyes by using Er³⁺: YAlO₃/TiO₂–SnO₂ under ultrasonic irradiation, *J. Mol. Catal. A Chem.* 366 (2013) 282–287.
- [39] M.A. Behnajady, N. Modirshahla, M. Shokri, B. Vahid, Effect of operational parameters on degradation of Malachite Green by ultrasonic irradiation, *Ultrason. Sonochem.* 15 (2008) 1009–1014.
- [40] E. Manousaki, E. Psillakis, N. Kalogerakis, D. Mantzavinos, Degradation of sodium dodecylbenzene sulfonate in water by ultrasonic irradiation, *Water Res.* 38 (2004) 3751–3759.
- [41] R. Marandi, M.E. Olya, B. Vahid, M. Khosravi, M. Hatami, Kinetic modeling of photocatalytic degradation of an azo dye using nano-TiO₂/polyester, *Environ. Eng. Sci.* 29 (2012) 957–963.
- [42] N. Ertugay, F.N. Acar, The degradation of Direct Blue 71 by sono, photo and sonophotocatalytic oxidation in the presence of ZnO nanocatalyst, *Appl. Surf. Sci.* 318 (2014) 121–126.
- [43] Y.L. Pang, A.Z. Abdullah, S. Bhatia, Review on sonochemical methods in the presence of catalysts and chemical additives for treatment of organic pollutants in wastewater, *Desalination* 277 (2011) 1–14.
- [44] N. Golash, P.R. Gogate, Degradation of dichlorvos containing wastewaters using sonochemical reactors, *Ultrason. Sonochem.* 19 (2012) 1051–1060.
- [45] J. Madhavan, P.S.S. Kumar, S. Anandan, F. Grieser, M. Ashokkumar, Degradation of acid red 88 by the combination of sonolysis and photocatalysis, *Sep. Purif. Technol.* 74 (2010) 336–341.
- [46] L. Hou, H. Zhang, L. Wang, L. Chen, Ultrasound-enhanced magnetite catalytic ozonation of tetracycline in water, *Chem. Eng. J.* 229 (2013) 577–584.
- [47] J. Wang, Z. Jiang, L. Zhang, P. Kang, Y. Xie, Y. Lv, R. Xu, X. Zhang, Sonocatalytic degradation of some dyestuffs and comparison of catalytic activities of nano-sized TiO₂, nano-sized ZnO and composite TiO₂/ZnO powders under ultrasonic irradiation, *Ultrason. Sonochem.* 16 (2009) 225–231.
- [48] A. Khataee, Y. Hanifehpour, M. Safarpour, M. Hosseini, S. Joo, Synthesis and characterization of Er_xZn_{1-x}Se nanoparticles: a novel visible light responsive photocatalyst, *Sci. Adv. Mater.* 5 (2013) 1074–1082.

- [49] A. Khataee, R. Darvishi Cheshmeh Soltani, Y. Hanifehpour, M. Safarpour, H. Gholipour Ranjbar, S.W. Joo, Synthesis and characterization of dysprosium-doped ZnO nanoparticles for photocatalysis of a textile dye under visible light irradiation, *Ind. Eng. Chem. Res.* 53 (2014) 1924–1932.
- [50] A. Khataee, A. Khataee, M. Fathinia, Y. Hanifehpour, S.W. Joo, Kinetics and mechanism of enhanced photocatalytic activity under visible light using synthesized $\text{Pr}_x\text{Cd}_{1-x}\text{Se}$ nanoparticles, *Ind. Eng. Chem. Res.* 52 (2013) 13357–13369.
- [51] X. Yan, J. He, D.G. Evans, X. Duan, Y. Zhu, Preparation, characterization and photocatalytic activity of Si-doped and rare earth-doped TiO_2 from mesoporous precursors, *Appl. Catal. B* 55 (2005) 243–252.
- [52] Z. Frontistis, D. Mantzavinos, Sonodegradation of 17α -ethynylestradiol in environmentally relevant matrices: laboratory-scale kinetic studies, *Ultrason. Sonochem.* 19 (2012) 77–84.
- [53] B. Gözmen, Applications of response surface analysis to the photocatalytic mineralization of acetaminophen over silver deposited TiO_2 with periodate, *Environ. Prog. Sustainable Energy* 31 (2012) 296–305.
- [54] B. Ervens, S. Gligorovski, H. Herrmann, Temperature-dependent rate constants for hydroxyl radical reactions with organic compounds in aqueous solutions, *Phys. Chem. Chem. Phys.* 5 (2003) 1811–1824.
- [55] M. Zarei, D. Salari, A. Niaei, A. Khataee, Peroxi-coagulation degradation of Cl Basic Yellow 2 based on carbon-PTFE and carbon nanotube-PTFE electrodes as cathode, *Electrochim. Acta* 54 (2009) 6651–6660.
- [56] A. Khataee, S. Arefi-Oskoui, A. Karimi, M. Fathinia, Y. Hanifehpour, S.W. Joo, Sonocatalysis of a sulfa drug using neodymium-doped lead selenide nanoparticles, *Ultrason. Sonochem.* 27 (2015) 345–358.